JOURNAL OF AIRCRAFT
Vol. 33, No. 2, March–April 1996

Aerodynamic Characteristics of a Two-Dimensional Airfoil with Ground Effect

Chih-Min Hsiun* and Cha'o-Kuang Chen†
National Cheng Kung University, Tainan 701, Taiwan, Republic of China

The effect of Reynolds number on the aerodynamic characteristics of an airfoil with ground effect in viscous flow is investigated by numerical method. A numerical scheme, based on the standard k-ε turbulence model, generalized body-fixed coordinates and the finite volume method, is developed to solve the two-dimensional wing-in-ground problem in viscous flow. The steady, incompressible Navier–Stokes equations are solved using a grid generation program developed by the authors, and the PHOENICS code. Some numerical results are presented to show the effects of Reynolds number, ground clearance, and angles of attack on the aerodynamic characteristics of a NACA 4412 airfoil.

Nomenclature

C_d = drag coefficient, $D/\frac{1}{2}\rho U_\infty^2 c$
C_l = lift coefficient, $L/\frac{1}{2}\rho U_\infty^2 c$
C_P = pressure coefficient, $(p - p_\infty)/\frac{1}{2}\rho U_\infty^2 c$
C = chord length of the airfoil
D = drag force
H = height of trailing edge of airfoil above ground
k = turbulent kinetic energy
L = lift force
$\bar{P}$ = grid control function
p = pressure
p_∞ = pressure at infinity
$\bar{Q}$ = grid control function
Re = Reynolds number, $U_\infty c/\nu$
U_∞ = freestream velocity
V_i = x component of velocity
V_j = y component of velocity
X = x-axis coordinate in physical domain
Y = y-axis coordinate in physical domain
α = angle of attack
ε = dissipation rate of turbulent kinetic energy
η = y-axis coordinate in computational domain
ν = kinematics viscosity
ξ = x-axis coordinate in computational domain

Introduction

THE phenomenon of special aerodynamic characteristics for an airfoil flying in close proximity to the ground is widely known as the wing-in-ground (WIG) effect. In general, the lift and drag forces of an airfoil will change considerably near ground. One important application of the WIG effect is the WIG vehicles that take off from and land on the water surface and cruise close to the water surface. Because of the WIG effect and its special operating environment, the aerodynamic characteristic of the WIG vehicle is an important design parameter. There were many theoretical and computational investigations of two-dimensional WIG problems in past years. For example, Widnall and Barrows[1] in 1970, developed an analytic solution for two- and three-dimensional wings in ground effects using the method of matched asymptotic expansions. Masuda and Suzuki[2] and Kataoka et al.[3] obtained some numerical results on the aerodynamic characteristics of a two-dimensional airfoil with free surface effect by panel method and discrete vortex method in 1991, respectively. In 1993, Nuhait and Zedan[4] investigated the unsteady problem of a flat plate with ground effect by the two-dimensional vortex–lattice method. Those numerical studies were based on an inviscid and incompressible flow assumption. In 1994, some numerical results of two-dimensional airfoils with ground effects in inviscid, compressible flow were presented by Morishita and Tezuka.[5] As for the viscous effect, Steinbach and Jacob[6] in 1991 gave some computational data of airfoils with ground effects at high Reynolds number by an iterative procedure including the panel method, boundary-layer integral method, and rear separation displacement model. In 1993, Hsiun and Chen[7] solved the steady, incompressible Navier–Stokes (N–S) equations and obtained some numerical results of an airfoil with ground effect in laminar flow. Hirata[8] also solved the N–S equations to simulate the viscous flow around a two-dimensional power-augmented ram wing with ground effect in 1993.

Some experimental results made by Hayashi and Endo[9] showed that, at lower Reynolds number ($Re = 3.2 \times 10^5$) and higher angles of attack, the flow separation phenomenon of the airfoil with ground effect was stronger than that without ground effect. In addition, they showed that the numerical method based on inviscid flow assumption had poorly predicted the lift force of the airfoil with ground effect for angles of attack larger than 5 deg. In some cases with lower Reynolds number, higher angles of attack, and a very small ground clearance (e.g., the WIG vehicles take off from the water surface and the case of a free-flight model of WIG vehicle with a small size), the viscous effect will influence the aerodynamic characteristics strongly and cannot be neglected. However, to the best of the authors' knowledge, there are few detailed studies of aerodynamic characteristics in this range. In this article, the Reynolds number effect on the aerodynamic characteristics (including lift, drag, and lift-to-drag ratio) of an airfoil with ground effect in viscous flow is studied by a numerical method. The two-dimensional, steady, incompressible Navier–Stokes equations are solved by the finite volume method with a standard two-equation turbulent model[10–12] to obtain the solution of the WIG problem. The effects of the Reynolds number, ground clearance, and the angle of attack on the performance of the airfoil are discussed.

Mathematical Model

Figure 1 shows the physical model of the two-dimensional WIG problem. In this article, the free surface effect is ne-

Received Dec. 30, 1994; revision received Sept. 20, 1995; accepted for publication Oct. 10, 1995.
*Graduate Student, Department of Mechanical Engineering.
†Professor, Department of Mechanical Engineering.

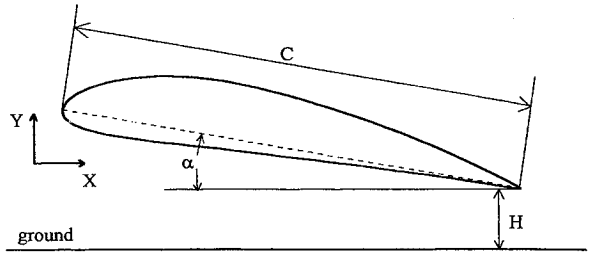

Fig. 1 Physical model of two-dimensional WIG problem.

glected. The equations governing the fluid flow are the steady, incompressible Navier–Stokes equations. The standard k-ε model is used. In Ref. 13, Rhie and Cho took the similar turbulent model to calculate the turbulent flow past an airfoil and they obtained good numerical results. The nondimensional Navier–Stokes equations, written in the nonconservative form, are

Continuity equation:

$$\frac{\partial}{\partial X_j} V_{j=0} \qquad j = 1, 2 \tag{1}$$

Momentum equation:

$$\frac{\partial}{\partial X_j}(V_i V_j) = -\frac{1}{\rho}\frac{\partial P}{\partial X_i} + \frac{1}{\rho}\frac{\partial}{\partial X_j}(\sigma_{ij}) \qquad i, j = 1, 2 \tag{2}$$

where V_i is the velocity component in the i direction and P and ρ are the pressure and density of fluid, respectively. The stress is given by

$$\sigma_{ij} = \mu_e \left(\frac{\partial V_i}{\partial X_j} + \frac{\partial V_j}{\partial X_i}\right) \tag{3}$$

where μ_e is the effect turbulent viscosity[12] and is given by

$$\mu_e = \mu + \mu_t = \mu + C_\mu \rho k^2/\varepsilon \tag{4}$$

μ and μ_t are the laminar and turbulent viscosity, respectively, C_μ is a constant, k is the turbulent kinetic energy, and ε is the dissipation rate of turbulent kinetic energy.

Transport equation for the turbulent kinetic energy is

$$\frac{\partial}{\partial X_j}(\rho V_j k) = \mu_t \left(\frac{\partial V_i}{\partial X_j} + \frac{\partial V_j}{\partial X_i}\right)\frac{\partial V_i}{\partial X_j} + \frac{\partial}{\partial X_j}\left(\frac{\mu_t}{\sigma_k}\frac{\partial k}{\partial X_j}\right) - \rho\varepsilon \tag{5}$$

Transport equation for the dissipation rate of turbulent kinetic energy is

$$\frac{\partial}{\partial X_j}(\rho V_j \varepsilon) = \frac{\partial}{\partial X_j}\left(\frac{\mu_t}{\sigma_\varepsilon}\frac{\partial \varepsilon}{\partial X_j}\right) + C_{1\varepsilon}\frac{\varepsilon}{k}\mu_t\left(\frac{\partial V_i}{\partial X_j} + \frac{\partial V_j}{\partial X_i}\right)\frac{\partial V_i}{\partial X_j} - C_{2\varepsilon}\rho\frac{\varepsilon^2}{k} \tag{6}$$

The values of previous constants C_D, $C_{1\varepsilon}$, $C_{2\varepsilon}$, and σ_ε are taken from Ref. 12 as $C_\mu = 0.09$, $C_{1\varepsilon} = 1.44$, $C_{2\varepsilon} = 1.92$, $\sigma_k = 1.0$, and $\sigma_\varepsilon = 1.23$.

The boundary conditions applied to this problem are as follows:

1) The velocity at upstream is uniform, that is $u = 1$ and $v = 0$ at infinity.

2) The velocity at external boundary is uniform, that is $u = 1$ and $v = 0$.

3) The no-slip condition is applied on the surface of the airfoil and the ground, that is $u = 0$ and $v = 0$.

4) The zero gradient condition is assumed for all variables at downstream boundary, that is $\partial u/\partial x = 0$ and $\partial v/\partial x = 0$.

The external boundary condition is $u = 1$ and $v = 0$ This condition is based on the hypothesis that the freestream is not influenced by the airfoil if the distance between the external boundary and the airfoil is large enough.

Numerical Scheme

Grid Generation

The curvilinear coordinate system is adopted to solve Eqs. (1–6) to accurately take into account the shape of the boundary. Consider the partial differential equations that define the mapping between a Cartesian coordinates region on the x, y plane (physical domain) and a region on the ξ, η plane (computational domain):

$$\xi_{xx} + \xi_{yy} = \bar{P} \tag{7}$$

$$\eta_{xx} + \eta_{yy} = \bar{Q} \tag{8}$$

where $\xi_{xx} = \partial^2\xi/\partial x^2, \ldots,$ $\bar{P}$ and $\bar{Q}$ are the control functions. By interchanging the dependent and independent variables, Eqs. (4) and (5) can be written as[14]

$$\bar{\alpha}x_{\xi\xi} - 2\bar{\beta}x_{\xi\eta} + \bar{\gamma}x_{\eta\eta} + \bar{J}^2(\bar{P}x_\xi + \bar{Q}x_\eta) = 0 \tag{9}$$

$$\bar{\alpha}y_{\xi\xi} - 2\bar{\beta}y_{\xi\eta} + \bar{\gamma}y_{\eta\eta} + \bar{J}^2(\bar{P}y_\xi + \bar{Q}y_\eta) = 0 \tag{10}$$

where

$$\begin{aligned} \bar{\alpha} &= x_\eta^2 + y_\eta^2 \\ \bar{\beta} &= x_\xi x_\eta + y_\xi y_\eta \\ \bar{\gamma} &= x_\xi^2 + y_\xi^2 \\ \bar{J} &= x_\xi y_\eta + x_\eta y_\xi \end{aligned} \tag{11}$$

To simplify the procedure of getting the results of Eqs. (9) and (10), the control functions $\bar{P}$ and $\bar{Q}$ are set to be zero. An H-type grid is used in this article and Fig. 2 shows the part of the grid mesh around the airfoil with ground effect.

Numerical Solver of N–S Equations

The set of conservation equations including Eqs. (1–6) can be rewritten in the curvilinear coordinate system by the general differential equation of the form

$$\nabla(\rho\phi V) - \nabla(\Gamma_\phi \nabla\phi) = S_\phi \tag{12}$$

where ϕ is the dependent variable to be computed, ρ is the density of the fluid, V is the velocity vector, Γ_ϕ is an exchange coefficient, and S_ϕ is a source term.

The first and second terms on the left side of Eq. (12) are the convection and diffusion terms, respectively.

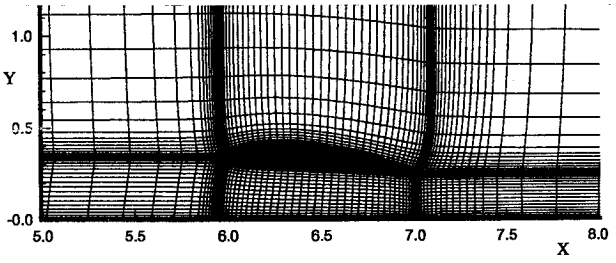

Fig. 2 Computational grid system with ground effect.

The finite volume approach is applied for discretizing the transformed governing equations as the type of Eq. (12). The combination of upwind and hybrid schemes is employed in the evaluation of the convection terms. The finite difference equations are obtained by integrating the transformed governing equations over individual control volumes formed by the staggered system. The variable P is located at the center of the control volume, while velocity components are positioned at the control volume face. The final form of the discretized governing equations are obtained:

$$a_P\phi_P = a_N\phi_N + a_S\phi_S + a_E\phi_E + a_W\phi_W + \bar{S}_\phi \qquad (13)$$

The subscript P refers to grid node to be considered and the other neighboring grids in the section are given by the subscripts N, S, E, and W. The a_N, a_S, a_E, and a_W represent the convection and diffusion coefficients at each corresponding control surface.

The SIMPLE[15] (semi-implicity pressure linked equation) method is applied to solve Eq. (13) and the dependent variables are iteratively solved until the converged solutions are obtained. The procedure is summarized as follows:

1) Construct the physical and computational grids system, and calculate $\bar{\alpha}$, $\bar{\beta}$, $\bar{\gamma}$, and $\bar{J}$ from Eq. (11).

2) Specify the initial conditions of the flowfield.

3) Solve the velocities with initial or previously calculated pressure.

4) Solve the pressure-correction equations.

5) Correct the pressure and velocities distributions of the flowfield.

6) Return to step 3 and repeat steps 3–6 until the residues are reduced to a special small value.

The overall solution procedure includes two parts: 1) the grid generation of the curvilinear coordinate system and 2) the finite volume numerical scheme applied to solve the conservation equations. In this article the PHOENICS[16] code is applied to solve the conservation equations and the grid mesh is obtained from a two-dimensional grid generation tool developed by the authors.

Results and Discussion

Comparison of Numerical and Experimental Results for the NACA 4412 Airfoil

The numerical results of the NACA 4412 airfoil at two different computational conditions are obtained by the present method and compared with the experimental data. The first computational case is the NACA 4412 airfoil at $\alpha = 8$ deg, $Re = 9 \times 10^5$, and without including ground effect. A total of 111 $\times$ 62 grids was used with 40 points distributed over one of the airfoil surfaces. The front and rear outer boundaries were located at 6 and 12 chord lengths away from the airfoil; the top and bottom outer boundaries were located at 6 chord lengths

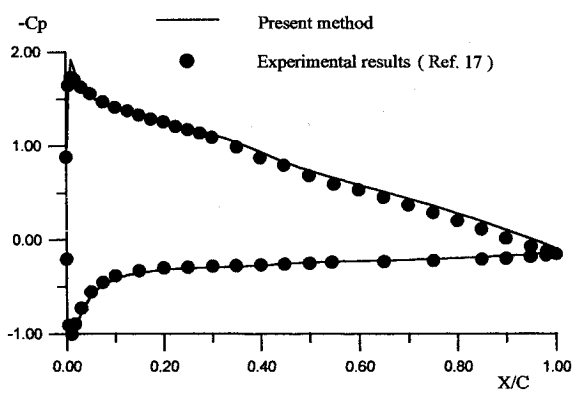

Fig. 3 Comparison of C_p curves of NACA 4412 airfoil without ground effect ($Re = 9 \times 10^5$, $\alpha = 8$ deg).

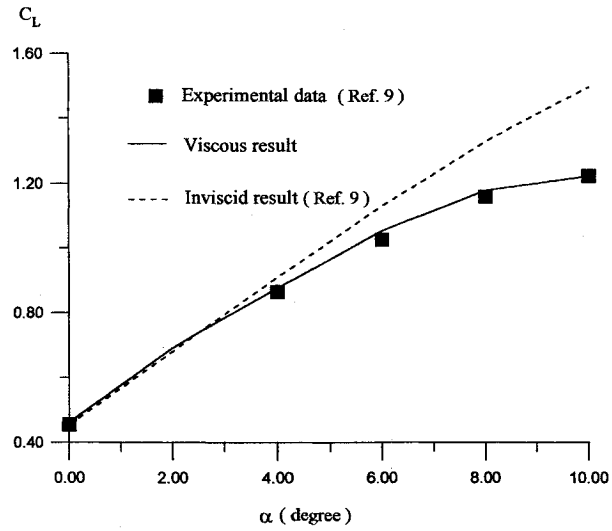

Fig. 4 Comparison of $C_l - \alpha$ curves of NACA 4412 airfoil with ground effect ($Re = 3.2 \times 10^5$, $H/C = 0.4$).

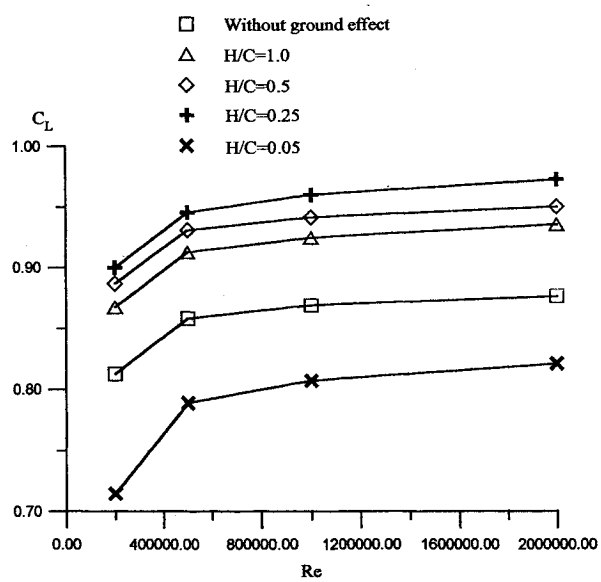

Fig. 5 Effect of Reynolds numbers on lift coefficient at $\alpha = 5$ deg.

from the airfoil. The numerical values of the surface pressure distribution obtained by the present method are compared with the measured values from Ref. 17 as shown in Fig 3. It shows that the numerical results of C_p on the lower surface have good consistency with the experimental data and the values of C_p on the upper surface near the trailing edge are slightly larger than those of the measured values.

The next computational case is the NACA 4412 airfoil with ground effect at $H/c = 0.4$ and $Re = 3.2 \times 10^5$. Figure 4 shows the comparison between the C_l values obtained from measurement,[9] an inviscid flow method,[9] and the present numerical method. In this case, H is the distance between ground and the midchord point of the airfoil. It is clear that the error between inviscid flow results and experimental data increases with increasing α. On the other hand, the viscous flow results obtained by the present method agree very well with the measured values. From the comparison previously mentioned, the capability of the present numerical procedure to solve the WIG problem in viscous flow can be proven.

Some numerical results obtained by the present method show the effect of Reynolds number on the aerodynamic characteristics of the airfoil with ground effect. The range of computational domain and grid mesh are the same as in the pre-

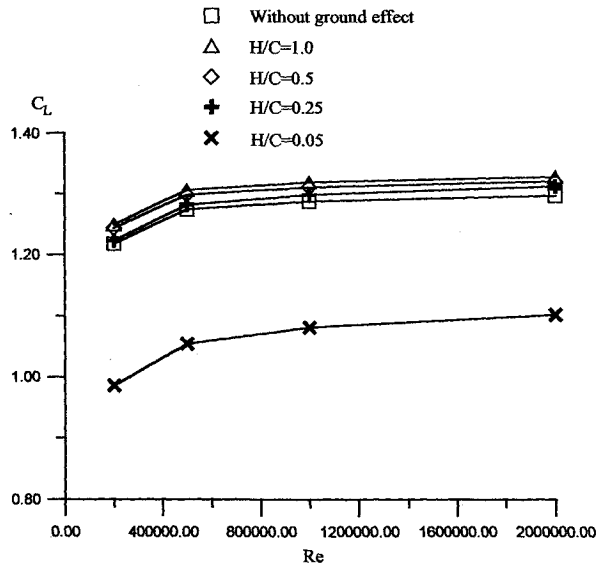

Fig. 6 Effect of Reynolds numbers on lift coefficient at α = 10 deg.

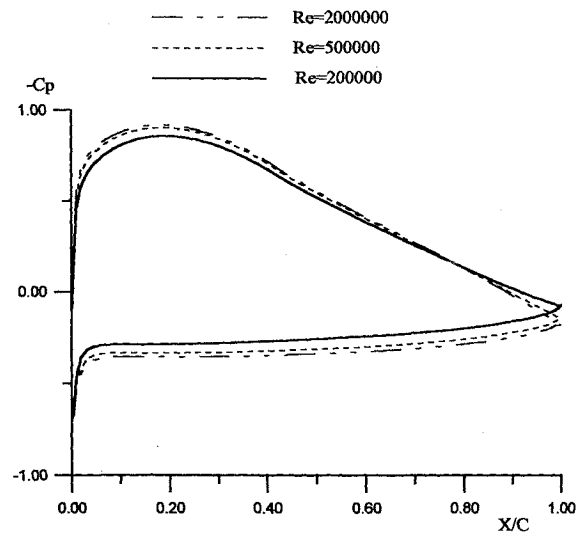

Fig. 7 Comparison of C_p curves for different *Re* (α = 5 deg, *H/C* = 0.25).

vious numerical cases. The flow over the NACA 4412 airfoil at α = 5 and 10 deg were calculated for $Re = 2 \times 10^5$, 5×10^5, 1×10^6, and 2×10^6. The values of *H/C* were fixed as 6.0 (without ground effect), 1.0, 0.5, 0.25, and 0.05. These results will be discussed next.

Effect of Reynolds Number for Airfoil with Ground Effect

The lift coefficients as a function of *Re* at α = 5 and 10 deg are shown in Figs. 5 and 6, respectively. It is clear that the lift coefficient increases with increasing *Re*. The relation between C_l and *Re* is not linear for $Re < 5 \times 10^5$. This trend is the same for all computed cases with or without ground effect. However, in Figs. 5 and 6, the slopes of $C_l - Re$ curves for the case of *H/C* = 0.05 are larger than those of other *H/C* cases. It indicates that the effect of Reynolds number on C_l is stronger at *H/C* = 0.05. Figures 7 and 8 show the comparisons of the surface pressure distribution at different Reynolds numbers with α = 5 deg, *H/C* = 0.05 and 0.25, respectively. Figures 7 and 8 show that the suction forces on the upper surface for all *Re* with *H/C* = 0.05 are smaller than those of *H/C* = 0.25. As for the effect of *Re* on C_P, it is clear that the pressure distribution on the upper surface at different *Re* have little difference when *H/C* = 0.25. On the other hand, the pressure distribution on the upper surface at $Re = 2 \times 10^5$ is very different from those of $Re = 5 \times 10^5$ and 2×10^6 for the case of *H/C* = 0.05. This result can be explained from the change of the ground boundary layer. Since the airfoil is very close to ground, *H/C* = 0.05, the mass of flow near the leading edge is also considerably less than that of the case with *H/C* = 0.25, and the suction force on the upper surface is smaller. This

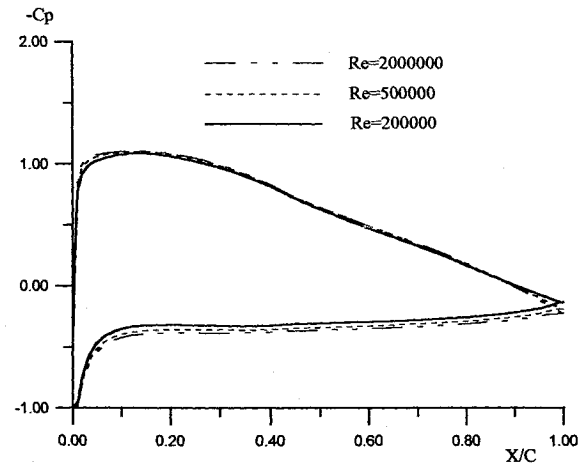

Fig. 8 Comparison of C_p curves for different *Re* (α = 5 deg, *H/C* = 0.25).

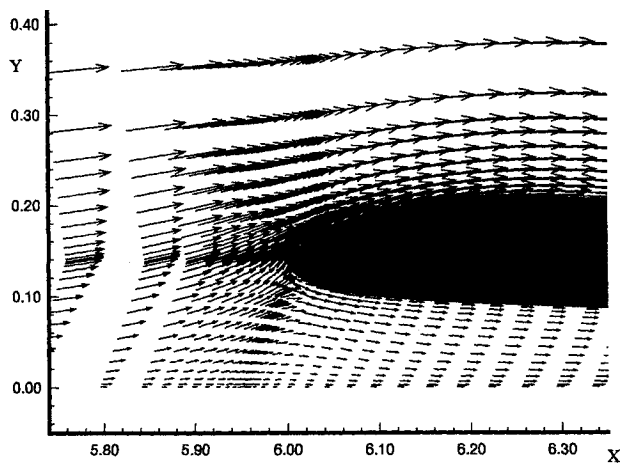

Fig. 9 Velocity vector around the leading edge of the airfoil ($Re = 2 \times 10^5$, α = 5 deg, and *H/C* = 0.05).

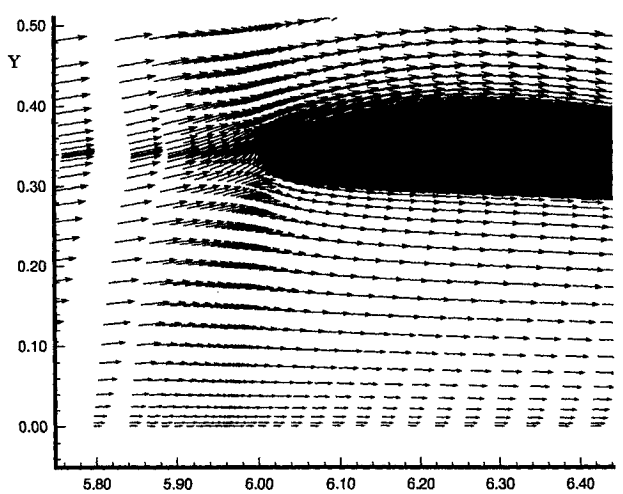

Fig. 10 Velocity vector around the leading edge of the airfoil ($Re = 2 \times 10^5$, α = 5 deg, and *H/C* = 0.25).

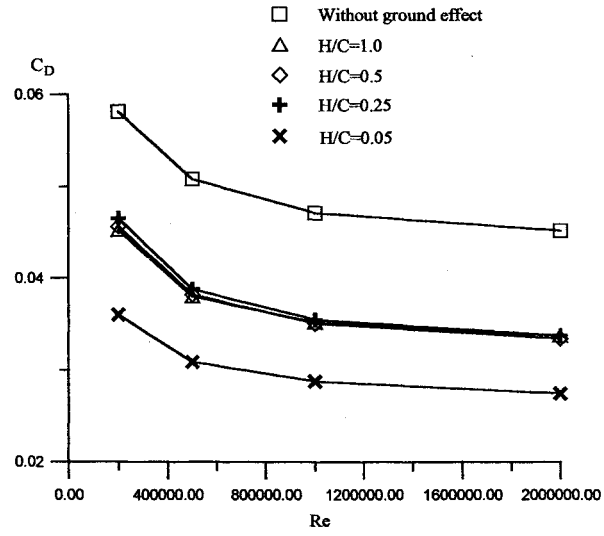

Fig. 11 Effect of Reynolds numbers on drag coefficient at α = 5 deg.

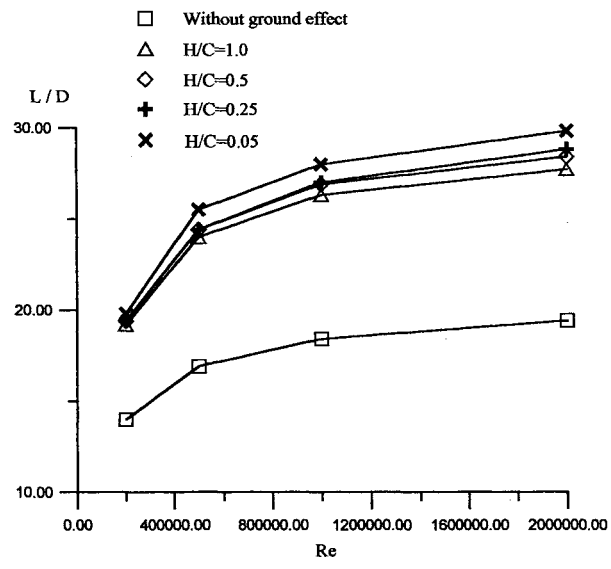

Fig. 12 Effect of Reynolds numbers on lift-to-drag ratio at α = 5 deg.

phenomenon can be illustrated using Figs. 9 and 10 showing the velocity vector around the leading edge of the airfoil with $Re = 2 \times 10^5$ and for $H/C = 0.05$ and 0.25, respectively. The velocity reducing effect because of the ground boundary layer can be shown clearly by comparing the two figures. Since the boundary-layer thickness increases with decreasing Re, the mass flow of fluid near the leading edge decreases. Hence, the pressure distribution on the leading edge is influenced more strongly at lower Reynolds number.

The effect of Re on drag coefficient at $\alpha = 5$ deg is shown in Fig. 11. The C_d value decreases with increasing Re because of the friction force coefficient decreasing and the ground effect decreases the drag coefficients for all Re. This is because of the decrease in pressure drag and will be explained later. The behavior of $C_d - Re$ curves at $\alpha = 10$ deg is the same as $\alpha = 5$ deg and is not shown. The effect of Re on lift-to-drag ratio is shown in Fig. 12. Re increases the lift-to-drag ratio and the slopes of $L/D - Re$ curves change rapidly for $Re < 5 \times 10^5$ for all H/C values. In general, the effect of Re on L/D increases with decreasing H/C. This trend is the same as for the effect of H/C on lift coefficient. Although the lift coefficient decreases with decreasing H/C as shown in Fig. 6, the drag coefficient also decreases with decreasing H/C as shown in Fig. 11. Hence, L/D increases with decreasing H/C.

Effect of Ground Clearance for Airfoil with Ground Effect

The numerical results previously mentioned are replotted to show the effect of ground clearance on the aerodynamic coefficients. The lift coefficient as a function of H/C with $Re = 2 \times 10^5$ and 2×10^6 and $\alpha = 5$ and 10 deg is shown in Fig. 13. There are two important phenomena existing. First, the lift coefficients increase with decreasing ground clearance and this effect of $\alpha = 5$ deg is larger than that of $\alpha = 10$ deg. That is, the lift decreases for increasing α. This result is similar to that obtained by Kataoka et al.,[3] based on the inviscid flow assumption. However, their results show that the lift coefficient increased to a very large value continuously, provided that the ground clearance decreased to a very small value. The present numerical results show that it is not true when the viscous effect is considered. This is the second important phenomenon existing in Fig. 13. For $\alpha = 5$ deg, with H/C smaller than 0.25, all of the lift coefficients of different Re decrease rapidly. For $\alpha = 10$ deg, lift coefficients decrease earlier when the H/C value is smaller than 1.0, and C_l of different Re also decrease rapidly as $H/C = 0.05$.

Figure 14 shows a comparison of the surface pressure distribution for different H/C values with $Re = 2 \times 10^5$ and $\alpha = 5$ deg. For $H/C = 0.25$, C_l increases because of the increase of the positive pressure under the airfoil. On the upper surface, the suction pressure increases slightly at the leading edge and decreases at other positions. When H/C decreases to 0.05, the

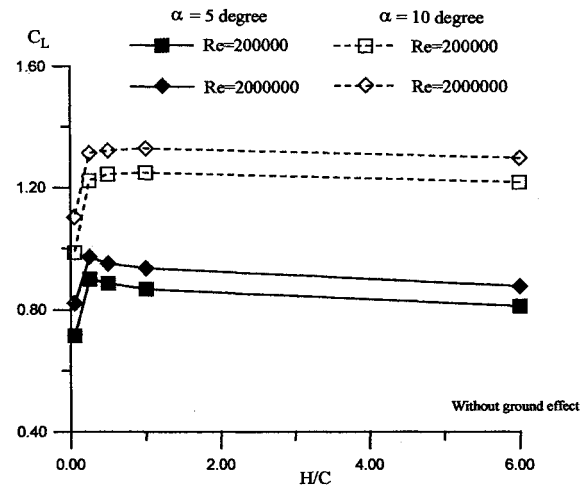

Fig. 13 Effect of H/C on lift coefficient.

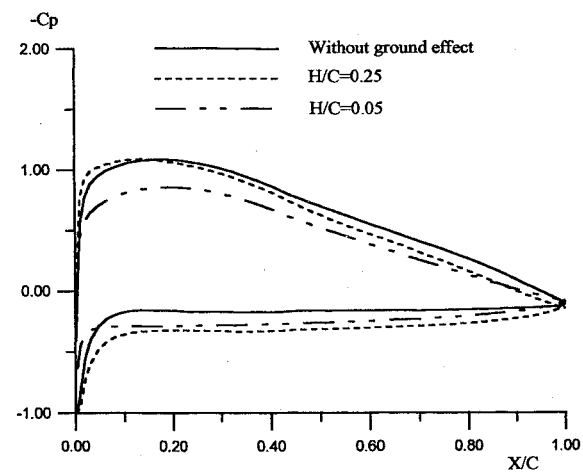

Fig. 14 Comparison of C_p curves for different H/C values ($Re = 2 \times 10^5$, $\alpha = 5$ deg).

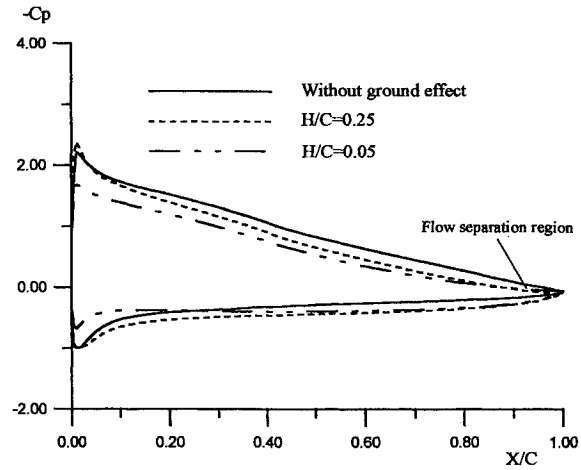

Fig. 15 Comparison of C_p curves for different H/C values (Re = 2×10^5, α = 10 deg).

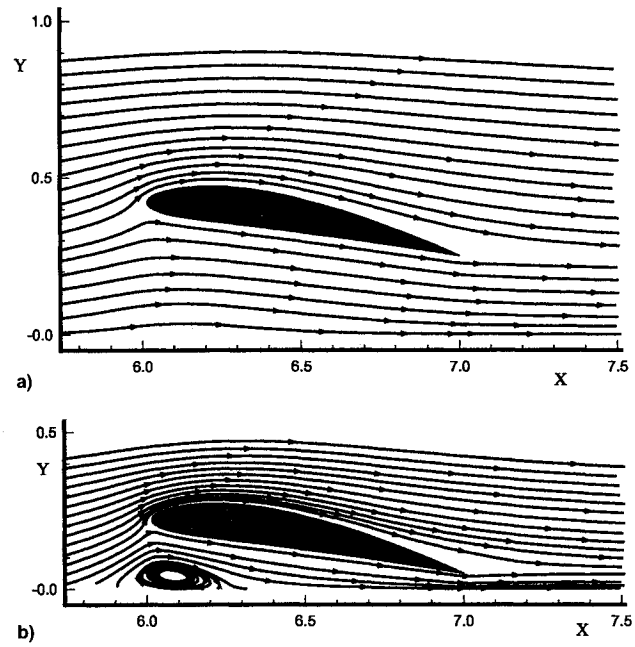

Fig. 16 Streamlines around the airfoil (Re = 2×10^5, α = 5 deg): H/C = a) 0.25 and b) 0.05.

positive pressure under the airfoil also increases, but the quantity is smaller than that of H/C = 0.25. At the same time, the suction pressure decreases rapidly when compared to that of H/C = 0.25, or the case without ground effect. This phenomenon is because of the effect of the ground boundary layer and can be seen in Figs. 9 and 10. Figure 15 is the comparison of the surface pressure distribution for different H/C values with $Re = 2 \times 10^5$ and α = 10 deg. Similar to the case with α = 5 deg, the ground effect increases the positive pressure under the airfoil and decreases the negative pressure on the upper surface. However, the loss of the suction force on the upper surface at α = 10 deg is larger than that of α = 5 deg; the flow separation at the trailing edge can be found for H/C = 0.25 and 0.05 cases when compared with the pressure distribution of the case without ground effect.

Another important phenomenon is the change of the lower surface pressure distribution near the leading edge. The reason is that some change of flowfield exists at that position. Figure 16 shows the streamlines around the airfoil for two values of ground clearance with $Re = 2 \times 10^5$ and α = 10 deg. In this figure, the phenomenon that the flow separated at the trailing edge can be found and a strong circular flow region generated between the leading edge and the ground for the case of H/C = 0.05. The similar circular flow region also can be found even for the case with $Re = 2 \times 10^6$. Since this circular flow region is not generated for H/C = 0.25 and for the cases with α = 5 deg. As a result, the generation of this circular flow region is because of the very small H/C value, the high angle of attack, and the viscous effect.

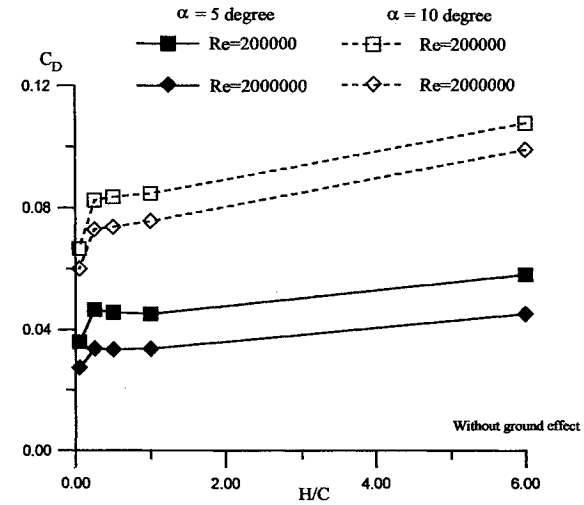

Fig. 17 Effect of H/C on drag coefficient.

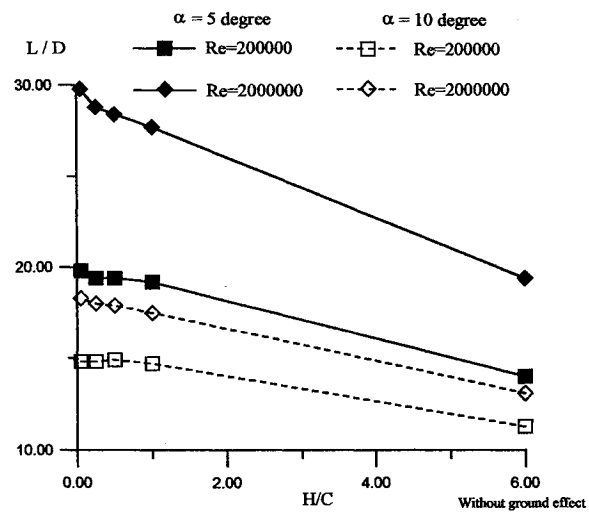

Fig. 18 Effect of H/C on lift-to-drag ratio.

The effect of the ground clearance on the drag coefficient for α = 5 and 10 deg with different Reynolds numbers is shown in Fig. 17. The ground effect decreases the drag coefficients for all cases with different Re and α. This result is because of the change of pressure drag of the airfoil with ground effect. In Figs. 14 and 15, the negative pressure on the upper surface of the airfoil decreases with the decreasing ground clearance and the pressure drag is reduced naturally. For the extreme case, H/C = 0.05, a larger loss of suction force above the airfoil causes a very small pressure drag. The drag coefficient will decrease rapidly for the case of H/C = 0.05, as shown in Fig. 17. As for the effect of the ground clearance on the lift-to-drag ratio, Fig. 18 shows that the ground effect increases the lift-to-drag ratio for all Re and α. This is because of the lift increasing and drag decreasing as the ground clearance decreasing, as mentioned previously.

Conclusions

A numerical procedure using the standard k-ε turbulence model and the finite volume method to solve the problem of a two-dimensional airfoil with ground effect in viscous flow is

developed in this work. The steady, incompressible Navier–Stokes equations are solved using the PHOENICS code and a grid generation program developed by the authors. Some cases of a WIG problem are calculated and the effects of the Reynolds number, the ground clearance, and the angle of attack on the aerodynamic characteristics of the airfoil are shown. Some conclusions are made from the present study:

1) A numerical procedure to solve the two-dimensional WIG problem with viscous effect is developed and has good capability to predicate the aerodynamic characteristics of the airfoil with ground effect at lower Reynolds numbers and higher α.

2) The lift coefficient increases with increasing *Re* and this effect is stronger for the case with very small ground clearance.

3) There is large loss of lift for the case with very small ground clearance because of the effect of the ground boundary layer.

4) For higher α and lower ground clearance, a strong circular flow region will generate at the position between the leading edge of the airfoil and the ground because of the viscous effect.

5) The drag coefficient decreases with decreasing ground clearance because of smaller pressure drag owing to the loss of suction force above the airfoil.

References

[1]Widnall, S. E., and Barrows, T. M., "An Analytic Solution for Two- and Three-Dimensional Wings in Ground Effect," *Journal of Fluid Mechanics*, Vol. 41, Pt. 4, 1970, pp. 769–792.

[2]Masuda, S., and Suzuki, K., "Simulation of Hydrodynamic Effects of 2-Dimensional WIG Moving near the Free Surface," *Journal of the Society of Naval Architects of Japan*, Vol. 170, Dec. 1991, pp. 83–92.

[3]Kataoka, K., Ando, J., and Nakatake, K., "Free Surface Effect on Characteristics of Two-Dimensional Wing," *Transactions of the West–Japan Society of Naval Architects*, No. 83, March 1991, pp. 21–30.

[4]Nuhait, A. O., and Zedan, M. F., "Numerical Simulation of Unsteady Flow Induced by a Flat Plate Moving Near Ground," *Journal of Aircraft*, Vol. 30, No. 5, 1993, pp. 611–617.

[5]Morishita, E., and Tezuka, K., "Ground Effect Calculation of Two-Dimensional Airfoil," *Trans. Japan Soc. Aero. Space Sci.*, Vol. 36, No. 114, 1994, pp. 270–280.

[6]Steinbach, D., and Jacob, K., "Some Aerodynamic Aspects of Wings near Ground," *Trans. Japan Soc. Aero. Space Sci.*, Vol. 34, No. 104, 1991, pp. 56–70.

[7]Hsiun, C. M., and Chen, C. K., "Numerical Calculation and Investigation of Aerodynamic Characteristics of Two-Dimensional Wing in Ground Effect," *6th National Conference on the Society of Naval Architects and Marine Engineering*, Society of Naval Architects and Marine Engineering of the Republic of China, Chia-Yi, Taiwan, ROC, 1993, pp. 1–12.

[8]Hirata, N., "Simulation on Viscous Flow around Two-Dimensional Power-Augmented Ram Wing in Ground Effect," *Journal of the Society of Naval Architects of Japan*, Vol. 174, Dec. 1993, pp. 47–54.

[9]Hayashi, M., and Endo, E., "Measurement of Flow Fields Around an Airfoil Section with Separation," *Trans. Japan Soc. Aero. Space Sci.*, Vol. 21, No. 52, 1978, pp. 69–75.

[10]Harlow, F. H., and Nakayama, P., "Transport of Turbulence Energy Decay Rate," Univ. of California, Los Alamos Science Lab., Rept. LA-3854, CA, 1968.

[11]Jones, W. P., and Launder, B. E., "The Prediction of Laminarization with a 2-Equation Model of Turbulence," *International Journal of Heat and Mass Transfer*, Vol. 15, No. 2, 1972, p. 301.

[12]Launder, B. E., and Spalding, D. B., "The Numerical Computation of Turbulent Flows," *Computer Methods in Applied Mechanics and Engineering*, Vol. 3, No. 2, 1974, pp. 269–289.

[13]Rhie, C. M., and Chow, W. L. "Numerical Study of the Turbulent Flow Past an Airfoil with Trailing Edge Separation," *AIAA Journal*, Vol. 21, No. 11, 1983, pp. 1525–1532.

[14]Thompson, J. F., Thames, F. C., and Mastin, C. W., "Automatic Numerical Generation of Body-Fitted Curvilinear Coordinate System for Field Containing Any Number of Arbitrary Two Dimensional Bodies," *Journal of Computational Physics*, Vol. 15, No. 3, 1974, pp. 299–319.

[15]Patankar, S. V., "Numerical Heat Transfer and Fluid Flow," McGraw–Hill, New York, 1980, pp. 120–129.

[16]Spalding, D. B., "PHOENICS Instruction Course," Concentration, Heat and Momentum Ltd., TR/300, London, 1987.

[17]Pinkerton, R. M., "The Variation with Reynolds Number of Pressure Distribution over an Airfoil Section," NACA Rept. 613, 1938, pp. 6–11.